CRYSTAL GROWTH & DESIGN
2007
VOL. 7, NO. 5
956−961

Effects of Reaction Gel Dehydration on the Synthesis of $Cu(NC_5H_5)_4VOF_4$ and $[Cu(NC_5H_5)_4VOF_4][Cu(NC_5H_5)_4(H_2O)VOF_4]\cdot H_2O$

Margaret E. Welk,‡ Charlotte L. Stern, Kenneth R. Poeppelmeier, and Alexander J. Norquist*,†

Department of Chemistry, Northwestern University, Evanston, Illinois 60208-3113

Received December 11, 2006

ABSTRACT: The acentric anion, $[VOF_4]^{2-}$, has been incorporated into two new compounds, $[Cu(NC_5H_5)_4VOF_4][Cu(NC_5H_5)_4(H_2O)VOF_4]\cdot H_2O$ and $Cu(NC_5H_5)_4VOF_4$. Single crystals of both compounds were grown from nearly identical reaction gels under mild hydro(solvo)thermal conditions, which differed only in the inclusion or exclusion of water. While both compounds contain infinite chains, stark differences in structure and composition are observed. The composition of $[VOF_4]^{2-}$ dictates the anion's geometry, structure-directing properties, and hydrogen-bonding capacity, and is responsible for the compositional variation between $[Cu(NC_5H_5)_4VOF_4][Cu(NC_5H_5)_4(H_2O)VOF_4]\cdot H_2O$ and $Cu(NC_5H_5)_4VOF_4$, the observed local and extended order of oxide fluoride anions, and unusual packing motifs. Primary coordination to each $[VOF_4]^{2-}$ anion in $[Cu(NC_5H_5)_4VOF_4][Cu(NC_5H_5)_4(H_2O)VOF_4]\cdot H_2O$ and $Cu(NC_5H_5)_4VOF_4$ is directed through *trans*-fluoride ligands, yet variability exists in further sites of interaction. Alignment of V−O bonds in $Cu(NC_5H_5)_4VOF_4$ results in concerted packing shifts and the destruction of intrachain centers of symmetry. The resulting noncentrosymmetric solid exhibits nonlinear optical activity; the second harmonic generation of $Cu(NC_5H_5)_4VOF_4$ was measured to be 20% of α-quartz using the Kurtz powder technique.

Introduction

"Bottom up" design of crystalline compounds has great potential for the creation of technologically important materials. Molecular or ionic components are chosen for their potential in the creation of new functional materials, which may exhibit interesting properties such as ferroelectricity, piezoelectricity, and second harmonic generation (SHG). For example, the early transition metal oxide fluoride anions $[NbOF_5]^{2-}$, $[TaOF_5]^{2-}$, and $[WO_2F_4]^{2-}$ are inherently acentric and polar, have polarizable metal−oxygen bonds, and are potential candidates for use in new SHG materials. Crystallization of these oxide fluoride anions in noncentrosymmetric structures has been the focus of several efforts.[1−3] Although the coordination preferences of these anions have been explored, the three-dimensional (3D) packing arrangements remain difficult to predict and control.[4,5]

Brock and others have developed a systematic grammar of crystal packing from statistical studies of existing crystal structure databases, in which several principles aid in understanding how a given crystal structure was formed.[6−12] Crystallization is generally directed so that (1) void spaces will be eliminated, (2) hydrogen-bond donors and acceptors will be satisfied, and (3) repulsive electrostatic interactions will tend to be minimized. The differences in structure and composition of two new compounds, $[Cu(NC_5H_5)_4VOF_4][Cu(NC_5H_5)_4(H_2O)VOF_4]\cdot H_2O$ (**1**) and $Cu(NC_5H_5)_4VOF_4$ (**2**), can be described using these rules. Infinite chains containing $[VOF_4]^{2-}$ anions show marked differences in packing and 3D symmetry with respect to the previously reported family $Cu(NC_5H_5)_4MX_6$ (MX_6 = $NbOF_5$, $TaOF_5$, WO_2F_4), which contains octahedral oxide fluoride anions.

* To whom correspondence should be addressed. E-mail: anorquis@haverford.edu.

† Present address: Department of Chemistry, Haverford College, Haverford, Pennsylvania 19041.

‡ Present address: Sandia National Laboratories, Department of Chemical and Biological Technologies, Albuquerque, New Mexico 87185-0734.

Experimental Section

Caution. $(HF)_x$·pyridine is toxic and corrosive!

Materials. CuO (99%, Aldrich), V_2O_4 (99.9%, Aldrich), pyridine (py, 99.8%, anhydrous, Aldrich), $(HF)_x$·pyridine (pyridine poly(hydrogen fluoride)), (70% HF by weight, Aldrich) were used as received. Reagent amounts of deionized H_2O were used.

Synthesis. Single crystals of **1** and **2** were prepared by placing the appropriate amount of reagents (see below) in Teflon (fluoro-ethylene-propylene) "pouches".[13] Several pouches with different reactant molar ratios (see Supporting Information) were sealed and placed into a Parr autoclave filled with 33% backfill (see below). The autoclave was sealed and heated at 150 °C for 24 h, and then cooled to room temperature over an additional 24 h. The pouches were removed from the autoclave and opened in air. Products were recovered by vacuum filtration.

$[Cu(py)_4VOF_4][Cu(py)_4(H_2O)VOF_4]\cdot H_2O$ (1). Single crystals of **1** were synthesized by placing 0.0575 g (7.23×10^{-4} mol) of CuO and 0.0600 g (3.61×10^{-4} mol) of V_2O_4 in a Teflon pouch. To the pouch were added 0.1989 g (7.55×10^{-4} mol) of $(HF)_x$·pyridine, 0.1011 g (5.62×10^{-3} mol) of H_2O, and 1.5066 g (1.90×10^{-2} mol) of pyridine. The 2000 mL Parr autoclave contained 667 mL of water used as backfill. Crystals of **1** were recovered as royal blue blocks in 62% yield based on copper. Decomposition of the crystals in air occurs after one week.

$Cu(py)_4VOF_4$ (2). Single crystals of **2** were synthesized by placing 0.0621 g (7.81×10^{-4} mol) of CuO and 0.0647 g (3.91×10^{-4} mol) of V_2O_4 in a Teflon pouch. To the pouch were added 0.1912 g (7.26×10^{-4} mol) of $(HF)_x$·pyridine and 1.5331 g (1.90×10^{-2} mol) of pyridine. The 125 mL Parr autoclave contained 41 mL of pyridine used as backfill. Crystals of **2** were recovered as dark blue blocks in 57% yield based on copper. Decomposition of crystals in air occurs within 2 days.

Crystallographic Determination. X-ray data were collected on a Bruker SMART 1000 CCD with the SMART[14] program. The SAINT-PLUS[15] program was used to integrate the diffraction frames. All calculations were performed using Crystals.[16] The structures were solved by direct methods[17] and expanded using Fourier techniques.[18] Data were corrected for absorption using the program SADABS.[19] All non-hydrogen atom sites were located from the difference map and refined using anisotropic thermal parameters. Hydrogen atoms H(26)−H(29) on the two water molecules in **1** were located from the difference maps. All other hydrogen atoms were placed as non-refined positions. See Tables 1 and 2 for relevant crystallographic data and selected bond lengths, respectively.

10.1021/cg0609062 CCC: $37.00
Published on Web 04/18/2007

Table 1. Crystallographic Data for $[Cu(py)_4VOF_4][Cu(py)_4(H_2O)VOF_4]\cdot H_2O$ and $Cu(py)_4VOF_4$

$[Cu(py)_4VOF_4][Cu(py)_4(H_2O)VOF_4]\cdot H_2O$ (**1**)	$Cu(py)_4VOF_4$ (**2**)
empirical formula:	empirical formula:
$C_{40}H_{44}Cu_2V_2N_8O_4F_8$	$C_{20}H_{20}CuVN_4OF_4$
fw 1081.80	fw 522.89
space group $P2_1/m$ (No. 11)	space group $C222_1$ (No. 20)
$a = 9.5464(7)$ Å	$a = 10.5023(5)$ Å
$b = 17.0621(11)$ Å	$b = 13.0806(7)$ Å
$c = 14.0941(10)$ Å	$c = 31.0970(16)$ Å
$\beta = 105.4560(10)^o$	
$V = 2212.6(3)$ Å^3	$V = 4272.0(4)$ Å^3
$Z = 2$	$Z = 8$
$T = 153(1)$ K	$T = 153(1)$ K
$\lambda = 0.71069$ Å	$\lambda = 0.71069$ Å
$\rho_{calc} = 1.622$ g/cm^3	$\rho_{calc} = 1.626$ g/cm^3
$\rho_{obsd}{}^a = 1.596(7)$ g/cm^3	$\rho_{obsd}{}^a = 1.616(5)$ g/cm^3
$\mu = 1.440$ mm^{-1}	$\mu = 1.487$ mm^{-1}
$R^b = 0.034$	$R^b = 0.028$
$R(F^2)_w{}^c = 0.076$	$R(F^2)_w{}^c = 0.067$

[a] Density measured by flotation pycnometry at 25 °C. [b] $R = \sum||F_o| - |F_c||/\sum|F_o|$. [c] $R(F^2)_w = [\sum w(|F_o^2| - |F_c^2|)^2/\sum w(F_o^2)^2]^{1/2}$.

Table 2. Selected Bond Lengths (Å) for 1 and 2

	$[Cu(py)_4VOF_4][Cu(py)_4(H_2O)VOF_4]\cdot H_2O$ (**1**)		
V1−O1	1.649(3)	V2−O2	1.623(3)
V1−F1	1.870(3)	V2−F4	1.848(3)
V1−F2	1.886(4)	V2−F5	1.9188(17)
V1−F3	1.730(3)	V2−F6	1.667(3)
Cu1−O1	2.209(3)	Cu2−F5	2.6356(17)
Cu−O4	2.981(4)		
	$Cu(py)_4VOF_4$ (**2**)		
V1−O1	1.598(3)	Cu1−F1	2.561(2)
V1−F1	1.952(2)	Cu1−F3	2.263(2)
V1−F2	1.877(2)		
V1−F3	1.815(2)		
V1−F4	1.857(3)		

Spectroscopic Measurements. Mid-infrared (400−4000 cm^{-1}) spectra were collected using a Bio-Rad FTS-60 FTIR spectrometer operating at a resolution of 2 cm^{-1}. The V−O stretch was visible at 905 cm^{-1} in the spectra of both **1** and **2**, as were the stretches for coordinated pyridine at 1537 and 1650 cm^{-1}. The stretch at 2300 cm^{-1} indicated water in the spectrum of **1**.

Susceptibility Measurements. The temperature dependence of the magnetic moment for single crystals of **2** (mass = 0.1006 g) was collected with a DC superconducting quantum interference device (SQUID) magnetometer from Quantum Design. After the sample was zero-field-cooled to 5 K, a 0.1 T field was applied, and the magnetic moment was registered. The susceptibility values were calculated per spin 1/2 ion from the magnetic moment data using the Curie−Weiss law to be μ(eff) = 1.60. This is very close to the expected value of 1.73, indicating that the two spin 1/2 species were isolated and non-interacting, and is consistent with the crystal structure which placed the Cu^{2+} (d^9) and V^{4+} (d^1) approximately 4.07 Å apart. Susceptibility values for **1** were impossible to collect accurately owing to loss of occluded water and rapid decomposition during the data collection.

Results

Compound **1** contains two independent chain types, which exhibit the formulas $Cu(py)_4VOF_4$ and $Cu(py)_4(H_2O)VOF_4$, respectively. See Figure 1. The $Cu(py)_4VOF_4$ chains are constructed from alternating $[Cu(py)_4]^{2+}$ cations and $[VOF_4]^{2-}$ anions. The four equatorial coordination sites on the Cu^{2+} centers are occupied by pyridine ligands, through distances of 2.046(2) × 2 and 2.047(3) Å × 2. The Jahn−Teller active axial sites are occupied by fluoride ligands from neighboring trigonal bipyramidal $[VOF_4]^{2-}$ anions. One oxide and three unique fluoride sites are observed in the $Cu(py)_4VOF_4$ chains, with V−O and V−F bond lengths of 1.667(3), 1.848(3), and 1.9188(17) Å × 2. The orientation of the V−O bonds in successive

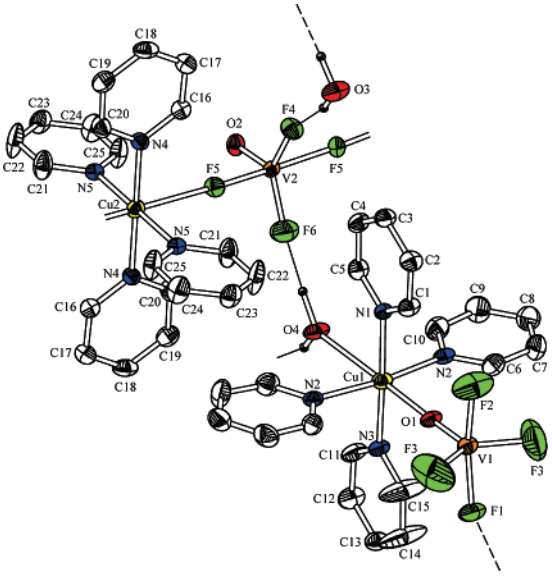

Figure 1. Thermal ellipsoid plot (50% probability) of $[Cu(py)_4VOF_4]$-$[Cu(py)_4(H_2O)VOF_4]\cdot H_2O$ (**1**). Dashed black lines denote hydrogen bonding. Hydrogen atoms are omitted for clarity.

$[VOF_4]^{2-}$ anions rotates 180 °, resulting in an "up−down−up" motif. See Figure 2a. These linear chains pack in parallel, 9.52 Å apart, to form layers in the *ab* plane. The pyridine rings in that plane participate in weak slipped $\pi-\pi$ stacking interactions with neighboring chains. The rings are separated by 3.87 Å.

The second chain type present in **1** exhibits a composition of $Cu(py)_4(H_2O)VOF_4$ and is constructed from discrete clusters that link to one another through a series of hydrogen bonds. These chains also contain $[Cu(py)_4]^{2+}$ cations, with similar Cu−N distances (2.044(4), 2.048(4) and 2.057(3) Å × 2), and $[VOF_4]^{2-}$ anions. However, each copper center is bound to one $[VOF_4]^{2-}$ anion through an oxide ligand and one bound water molecule through distances of 2.209(3) and 2.981(4) Å, as opposed to the two Cu−F−V connections in the first chain type. The $[VOF_4]^{2-}$ anions present in the $Cu(py)_4(H_2O)VOF_4$ chains are distorted trigonal bipyramids, with V−F bonds of 1.730(3) × 2, 1.870(3), and 1.886(4) Å. The bound water molecules donate hydrogen bonds to fluoride ligands on neighboring clusters, forming the second chain type. See Figure 2b. Coordinated pyridine rings participate in slipped $\pi-\pi$ stacking in the *ab* plane at a distance of 3.70 Å. See Figure 3. Additional hydrogen bonds are donated to nucleophilic fluorides on adjacent $Cu(py)_4VOF_4$ chains. The $Cu(py)_4(H_2O)VOF_4$ chains pack in puckered layers between layers of line $Cu(py)_4VOF_4$ chains. Both occluded (O3) and bound water molecules (O4) donate one hydrogen bond to each type of chain in **1**, creating an extensive 3D hydrogen-bonding network.

Compound **2** contains one-dimensional chains with the formula $Cu(py)_4VOF_4$. The chains are constructed from alternating $[Cu(py)_4]^{2+}$ cations and $[VOF_4]^{2-}$ anions, which are bound to one another through shared fluoride anions. See Figure 3. The four equatorial coordination sites on the copper center are occupied by pyridine ligands, through distances of 2.027(3), 2.032(3), 2.042(3), and 2.042(3) Å. The two axial Cu−F distances are 2.263(2) and 2.562(2) Å. The geometry of the $[VOF_4]^{2-}$ anion is square pyramidal, with V−F distances of 1.815(2), 1.857(3), 1.877(2), and 1.925(2) Å. The V−O distance is 1.598(3) Å.

The orientations of all the V−O bonds in a given chain are aligned. See Figure 4. Additionally, successive chains lie parallel to one another in the *ab* plane. The orientation of the chains

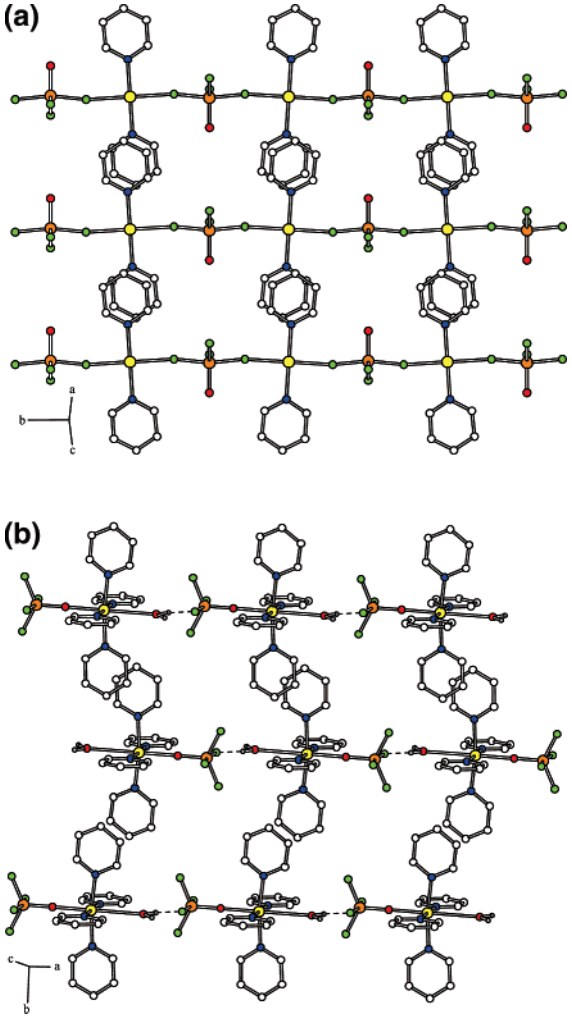

Figure 2. (a) $Cu(py)_4VOF_4$ chains and (b) hydrogen-bonded $Cu(py)_4(H_2O)VOF_4$ clusters in **1**. Yellow, orange, red, green, blue, and white circles represent copper, vanadium, oxygen, fluorine, nitrogen, and carbon, respectively. Selected pyridine rings and non-water hydrogen atoms are omitted for clarity. Dashed black lines denote hydrogen bonding.

within each layer is preserved; all V−O bonds have the same direction in each layer of chains.

The direction of chain propagation alternates between [1 1 0] and [1 $\bar{1}$ 0] every *c*/2, with neighboring chains being related to one another through a series of 2_1 screw axes. This results in crystallization in a nonpolar noncentrosymmetric space group ($C222_1$, No. 20) and the net cancellation of the V−O bond vectors in the solid. The 3D packing of **2** is shown in Figure 5b. The nonlinear optical activity of **2** was probed to confirm the space group assignment by measuring the SHG using the Kurtz powder technique. A response of approximately 20% of α-quartz was observed. This low response was anticipated, owing to the cancellation of the V−O bond axis vector and nonpolar crystal class, 222.[20,21]

Discussion

Short-range interactions between solvated molecules or ions that lead to crystallization are thought to be governed by a few simple rules. In order of importance, the species that crystallize will (1) attempt to eliminate void space,[6] (2) satisfy hydrogen-bond donors and acceptors and other intermolecular interactions where possible,[7−10] and (3) minimize electrostatic interactions.[6,12] The differences in structure and composition between **1** and **2** can be understood and explained in the context of these rules.

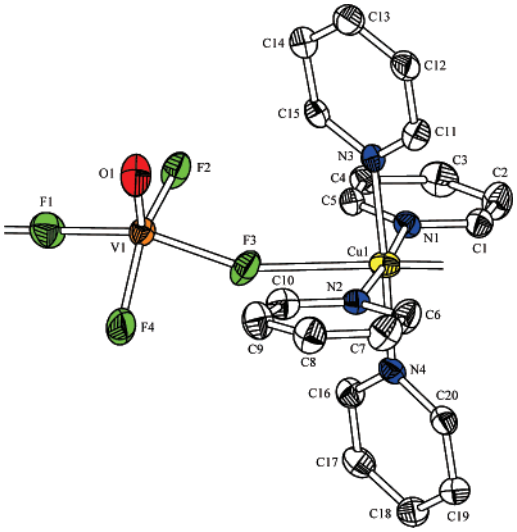

Figure 3. Thermal ellipsoid plot (50% probability) of $Cu(py)_4VOF_4$ (**2**). Hydrogen atoms are omitted for clarity.

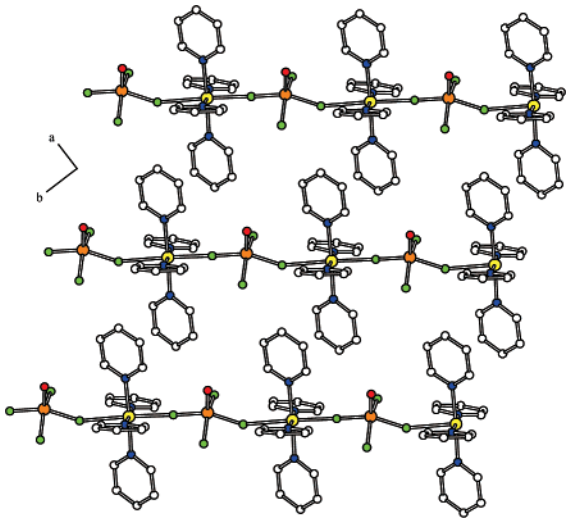

Figure 4. One layer of linear chains in **2**. Yellow, orange, red, green, blue, and white circles represent copper, vanadium, oxygen, fluorine, nitrogen, and carbon, respectively. Hydrogen atoms are removed for clarity.

The number of moles of CuO, V_2O_4, $(HF)_x$·pyridine, and pyridine remained approximately constant for the syntheses of **1** and **2**, while only the inclusion or exclusion of water varied. Despite the strong similarities in the reactions gels, these compounds show marked differences in structure and composition. The synthesis of **1** does not require the presence of water in the reaction pouch prior to reaction but does require that water be used to "backfill" the autoclave and counter the pressure generated inside of each pouch. The synthesis of **1** from reaction pouches that do not contain water relies upon the permeability of the Teflon pouch to water at elevated temperatures, at which point the backfill water can migrate into the reaction pouches and be incorporated in the reaction products. In contrast, the synthesis of **2** requires that water be used neither as a reagent in the reaction pouches nor as the backfill liquid. **2** was only formed when no water was added to the reaction pouch, *and* when pyridine was used as the backfill liquid. Only through

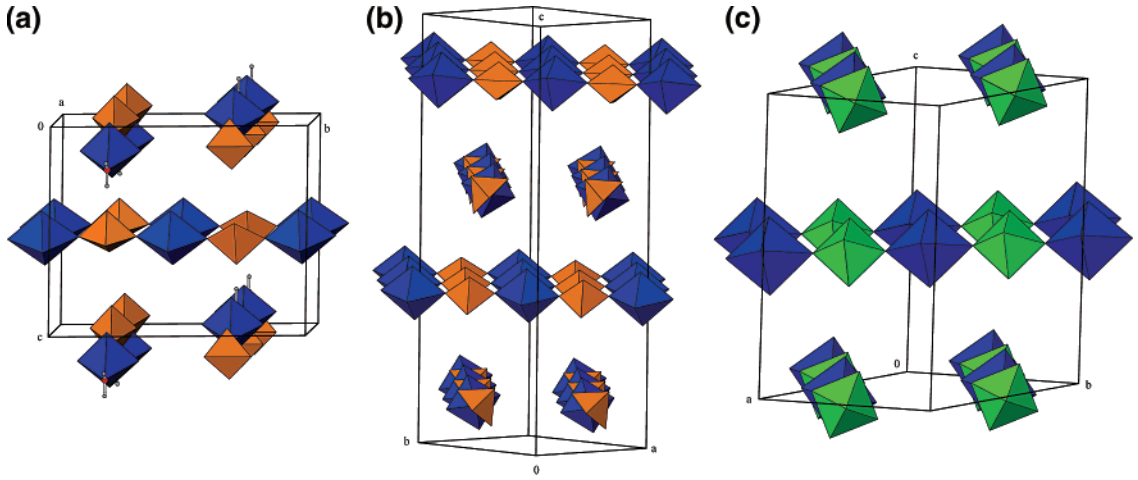

Figure 5. Packing diagram of (a) **1**, (b) **2**, and (c) $Cu(py)_4NbOF_5$. Blue, orange, and green polyhedra represent $[Cu(py)_4]^{2+}$, $[VOF_4]^{2-}$, and $[NbOF_5]^{2-}$, respectively.

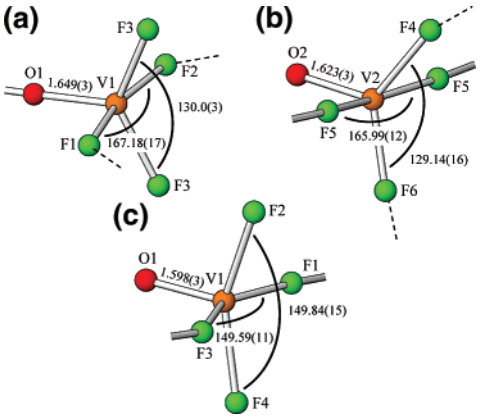

Figure 6. The $[VOF_4]^{2-}$ anions observed in (a) the $Cu(py)_4(H_2O)VOF_4$ clusters in **1**, (b) the $Cu(py)_4VOF_4$ chains in **1**, and (c) the $Cu(py)_4VOF_4$ chains in **2**. Selected bond lengths (Å) and angles (°) are shown. Cu−O and Cu−F connections are shown as thick bonds, while hydrogen bonds are shown as dashed lines.

the complete exclusion of liquid water from the pressure vessel, can the "non-hydrated" compound be formed. The permeability of the pouches to solvent migration at elevated temperatures is well-known and has been used in the low-temperature hydrothermal synthesis of delafossite-type oxides.[22−24]

The ease at which water is incorporated into **1** is related to its hydrogen-bonding affinity. Compound **2** is formed when water is absent and adopts a structure that contains many hydrogen-bond acceptors but no donors. The introduction of water to the reaction gel, either through direct addition to the pouch or through diffusion across the Teflon membrane, enables the formation of hydrogen bonds by providing a source of donors. Despite having nearly identical amounts of CuO, V_2O_4, $(HF)_x$·pyridine, and pyridine, a shift in reaction product from **2** to **1** is clearly observed after the introduction of water because the many fluoride and oxide ligands in **1** and **2** make ideal hydrogen-bond acceptors, which stabilize the structure.

The structural differences between **1** and **2** are not limited to the presence or absence of water. Distinct differences in $[VOF_4]^{2-}$ geometry and mode of attachment to neighboring copper centers are observed. See Figure 6. Compound **1** contains two unique $[VOF_4]^{2-}$ anions, both of which have distorted trigonal bipyramidal geometries. One anion is bound to a copper center through its oxide ligand, forming the $Cu(py)_4(H_2O)VOF_4$ clusters, while the other is bound to two neighboring copper centers through *trans*-fluoride ligands, forming the $Cu(py)_4VOF_4$ chains. Compound **2** contains a single type of $[VOF_4]^{2-}$ anion, in the form of a roughly square pyramid that is bound to two adjacent copper centers through *trans*-fluoride ligands.

The VO^{2+} bonds present in each anion are well-known to exhibit short distances, owing to significant oxygen to vanadium π-bonding.[25] The presence of a short V−O bond in the $[VOF_4]^{2-}$ coordination sphere induces a strong distortion of the vanadium center toward the lone oxide ligand, given that no analogous fluoride to vanadium π-bonding is observed. This "primary" distortion is solely a result of orbital overlap between the vanadium center and oxide ligand. Such distortions in oxide fluorides are well-known.[5,26,27]

Despite the presence of primary V−O distortions in each of the three unique $[VOF_4]^{2-}$ anions present in **1** and **2**, marked differences in V−O bond lengths are observed. See Figure 6. The longest V−O bond (1.649(3) Å) contains the only bridging oxide ligand present in **1** and **2**, while the two $V-O_{terminal}$ bonds are significantly shorter (1.598(3) and 1.623(3) Å). This difference is a result of a secondary distortion, caused by the bonding network surrounding the $[VOF_4]^{2-}$ anion. The V−O bond, shown in Figure 6a, is weakened and lengthened by the formation of a Cu−O bond. No such secondary distortions along the V−O bond axis are observed in the oxide ligands shown in Figure 6b,c. These ligands remain terminal, neither coordinating to an additional metal center nor participating in any hydrogen bonding.

The detection of a secondary distortion along the V−O bond axis in **1** is rare for two reasons. First, while primary and secondary distortions are common in early transition metal oxide fluoride anions (such as $[VOF_5]^{2-}$, $[NbOF_5]^{2-}$, $[TaOF_5]^{2-}$, $[MoO_2F_4]^{2-}$, and $[WO_2F_4]^{2-}$), crystallographic disorder of the oxide fluoride anions is rife.[1] This precludes the determination of true bond lengths and angles and makes a direct observation of any distortion impossible. However, primary distortions are readily observed in crystallographically ordered anions. Second, the structure directing properties of these anions dictate that interactions with surrounding species occur through the same ligands. For example, in the $[NbOF_5]^{2-}$ anion the first two ligands to participate in bonding are always the oxide and *trans*-fluoride, the same bonds in which the primary distortion is present.

A secondary distortion is observed in the $[VOF_4]^{2-}$ anion in **1** because the anion is crystallographically ordered and because the structure-directing properties of the anion are relaxed with

respect to analogous octahedral anions. The $[VOF_4]^{2-}$ anions in **2** are crystallographically ordered because they lack a sixth ligand, making interchain interactions more likely (see below). The oxide and fluoride ligands in $[NbOF_5]^{2-}$, $[TaOF_5]^{2-}$, and $[WO_2F_4]^{2-}$ tend to form regular octahedra, while their respective metal centers show small (~0.2 Å) deviations from the centers of their coordination octahedra. Much larger distortions are present in $[VOF_4]^{2-}$, where the absence of a sixth ligand increases the overall accentricity of the anions and deters disorder. In contrast to many other oxide fluoride anions, the structure-directing properties of $[VOF_4]^{2-}$ neither require nor preclude coordination to the oxide ligand. While primary coordination to $[VOF_4]^{2-}$ is directed through two *trans*-fluorides, additional interactions can occur through any of the other three ligands. Examples of coordination to each of the three remaining ligands are found in compounds **1** and **2** alone, allowing a direct observation of the secondary distortion along the V−O bond axis as shown in Figure 6a.

The composition, structure, and packing of **2** are analogous to the $Cu(py)_4MX_6$ (MX_6 = $NbOF_5$, $TaOF_5$, WO_2F_4) family of compounds. See Figure 5. Both **2** and the $Cu(py)_4MX_6$ compounds contain $[Cu(py)_4]^{2+}$ cations and either $[VOF_4]^{2-}$ or $[MX_6]^{2-}$ anions, from which infinite chains of alternating anions and cations are constructed. In each compound, successive layers of aligned chains are rotated 90° every *c*/2. The unit cell of the monoclinic $Cu(py)_4MX_6$ structure is related to the orthorhombic structure of **2** by the following relationship: $a_o = a_m$, $b_o = b_m$, $c_o = 2c_m \sin\beta_m$, where the subscripts o and m refer to the orthorhombic and monoclinic cells, respectively. The 3D packing of **2** and $Cu(py)_4NbOF_5$ is shown in Figure 7. Despite many similarities, several important differences exist. First, the spacings between adjacent layers in **2** alternate between 7.33 and 8.22 Å, while $Cu(py)_4NbOF_5$ has a single interlayer spacing of 7.98 Å. Second, the orientation of all V−O bonds in a given layer are aligned in ordered anions, while the $[MX_6]^{2-}$ anions are crystallographically disordered. Third, **2** crystallizes in the noncentrosymmetric space group $C222_1$ (No. 20), while the $Cu(py)_4MX_6$ compounds crystallize in the centrosymmetric space group *C*2/*c* (No. 15). Each of these dissimilarities shares the same root cause, the absence of a sixth ligand in the $[VOF_4]^{2-}$ anion.

Pyridine rings occupy much of the space between successive chains in both **2** and $Cu(py)_4MX_6$. See Figure 7. The oxide and fluoride ligands in $Cu(py)_4MX_6$ form a nearly regular octahedron, resulting in the formation of regular interlayer spacings (7.98 Å) and environments in $Cu(py)_4MX_6$. In contrast, the $[VOF_4]^{2-}$ anions exhibit distorted square pyramidal geometries. The absence of a sixth ligand in $[VOF_4]^{2-}$ creates small "pockets" within the structure, which are filled by nearby pyridine rings. Each V−O bond in a given layer is aligned (See Figures 4 and 7a) to allow for a concerted contraction of alternate interlayer spacing. That is, two adjacent layers move toward one another so that the "pockets" on each layer will be filled. This results in "short" distances of 7.33 Å between layers in which the V−O bonds are pointed away, and "long" distances of 8.22 Å in layers where the V−O bonds are pointed into the spacing. This asymmetry is responsible for the crystallographic ordering of the $[VOF_4]^{2-}$ anions in **2**.

The prevalence of crystallographic disorder within $[MX_6]^{2-}$ anions in $Cu(py)_4MX_6$ compounds as is a result of little interaction between neighboring chains, despite the presence of intraoctahedral distortions of within each $[MX_6]^{2-}$ anions. Solid-state ^{93}Nb, ^{19}F, and ^{113}Cd NMR on $Cd(py)_4NbOF_5$, an analogous compound that is isostructural to $Cu(py)_4MX_6$ (MX_6 = $NbOF_5$, $TaOF_5$, WO_2F_4), was used show that oxide and fluoride ligands are ordered within a given chain but disordered between neighboring chains.[28] The chemical constraints created by local order within a given chain are insufficient to enforce long range order, and an average structure (with imposed centers of symmetry) is visualized from bulk diffraction techniques.[29] These compounds, while they contain locally ordered chains, are crystallographically disordered and crystallize in the centrosymmetric group *C*2/*c* (No. 15). In contrast to $Cu(py)_4MX_6$ compounds, direct interaction between neighboring chains results in crystallographic order of the $[VOF_4]^{2-}$ anions in $Cu(py)_4VOF_4$.

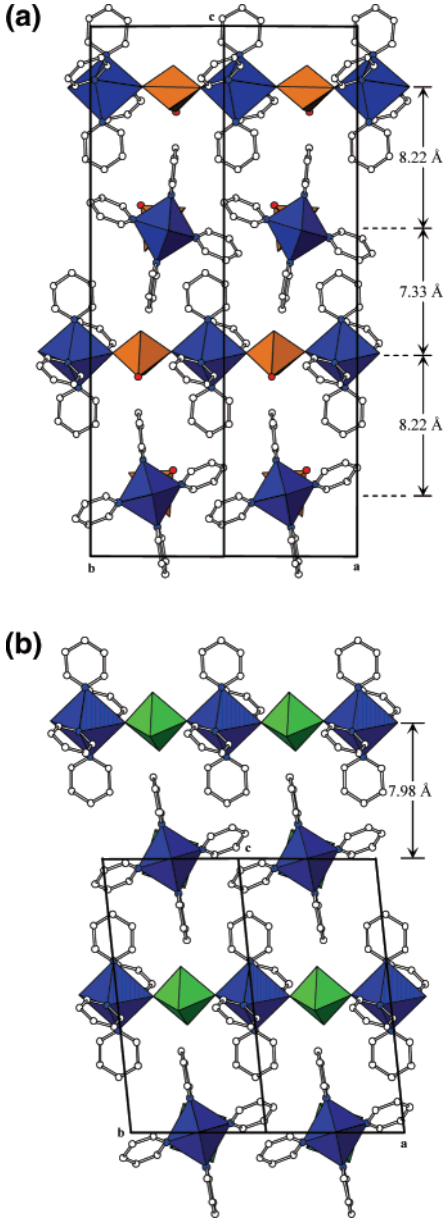

Figure 7. Unit cell packing of (a) **2** and (b) $Cu(py)_4NbOF_5$. Selected interlayer spacings are shown (Å). Blue, orange, and green polyhedra represent $[Cu(py)_4]^{2+}$, $[VOF_4]^{2-}$, and $[NbOF_5]^{2-}$, respectively. Blue, red, and white circles represent nitrogen, oxygen, and carbon atoms, respectively. Hydrogen atoms are removed for clarity.

Alignment of the V−O bonds in a given layer of chains allows for the contraction of the **2** lattice described above. In addition, this alignment affects the 3D symmetry of **2**, when compared to $Cu(py)_4NbOF_5$. Adjacent $Cu(py)_4NbOF_5$ chains are related to one another through a series of inversion centers, while

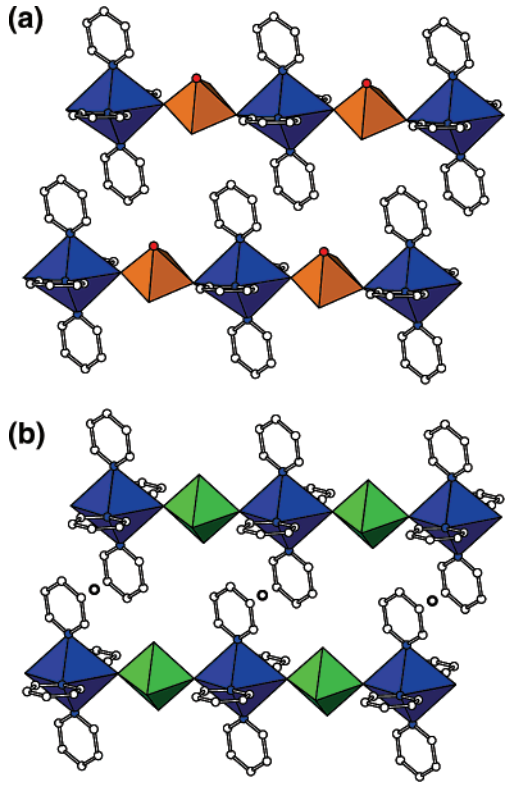

Figure 8. (a) $Cu(py)_4VOF_4$ and (b) $Cu(py)_4NbOF_5$ chains, with selected symmetry elements included. Blue, orange, and green polyhedra represent $[Cu(py)_4]^{2+}$, $[VOF_4]^{2-}$, and $[NbOF_5]^{2-}$, respectively. Blue, red, and white circles represent nitrogen, oxygen, and carbon atoms, respectively. Hydrogen atoms are removed for clarity.

no such centers of symmetry are present between $Cu(py)_4VOF_4$ chains in **2**. See Figure 8. The imposition of inversion centers between $Cu(py)_4VOF_4$ chains is prohibited by this anion alignment. Furthermore, the regular layer stacking observed in $Cu(py)_4NbOF_5$ is absent in **2**. See Figure 7. The interlayer spacings are not chemically identical in **2**, resulting in the formation of an alternate packing motif. The reduced symmetry of **2** is demonstrated in its noncentrosymmetric space group $C222_1$ (No. 20), the assignment of which was confirmed through the detection of nonlinear optical activity in the form of SHG.

Conclusion

The differences in structure and composition of $[Cu(NC_5H_5)_4VOF_4][Cu(NC_5H_5)_4(H_2O)VOF_4]\cdot H_2O$ and $Cu(NC_5H_5)_4VOF_4$ are directly related to the presence or absence of water from the structure. The use of $[VOF_4]^{2-}$, which exhibits similar structure directing properties as the $[MX_6]^{2-}$ anions in $Cu(py)_4MX_6$, enabled the determination of how changes in local anion structure affect long-range packing. The alignment of V−O bonds in **2** allows for the contraction of alternate interlayer spacings, which serve to eliminate the small void spaces behind each $[VOF_4]^{2-}$ anion. The noncentrosymmetry of **2** is directly dependent upon both the $[VOF_4]^{2-}$ alignment and asymmetry in layer stacking.

Acknowledgment. The authors thank Prof. P. Shiv Halasyamani at the University of Texas−Houston for the SHG data on $Cu(py)_4VOF_4$. The authors gratefully acknowledge support from the National Science Foundation, Solid-state Chemistry (Award No. DMR-0604454), and made use of Central Facilities supported by the MRSEC program of the National Science Foundation (Grant DMR-0076097 and DMR-0540513) at the Materials Research Center of Northwestern University.

Supporting Information Available: Two X-ray crystallographic files in CIF format including complete tables of crystallographic details, atomic coordinates, anisotropic thermal parameters, and interatomic distances and angles are available free of charge via the Internet at http://pubs.acs.org.

References

(1) Heier, K. R.; Norquist, A. J.; Wilson, C. G.; Stern, C. L.; Poeppelmeier, K. R. *Inorg. Chem.* **1998**, *37*, 76.
(2) Heier, K. R.; Norquist, A. J.; Halasyamani, P. S.; Duarte, A.; Stern, C. L.; Poeppelmeier, K. R. *Inorg. Chem.* **1999**, *38*, 762.
(3) Norquist, A. J.; Stern, C. L.; Poeppelmeier, K. R. *Inorg. Chem.* **1999**, *38*, 3448.
(4) Norquist, A. J.; Heier, K. R.; Stern, C. L.; Poeppelmeier, K. R. *Inorg. Chem.* **1998**, *37*, 6495.
(5) Welk, M. E.; Norquist, A. J.; Stern, C. L.; Poeppelmeier, K. R. *Inorg. Chem.* **2001**, *40*, 5479.
(6) Brock, C. P.; Dunitz, J. D. *Chem. Mater.* **1994**, *6*, 1118.
(7) Kitaigorodskii, A. I. *Organic Chemical Crystallography*; Consultant's Bureau: New York, 1961.
(8) Etter, M. C. *J. Phys. Chem.* **1991**, *95*, 4601.
(9) Donohue, J. *J. Phys. Chem.* **1952**, *56*, 502.
(10) Etter, M. C. *J. Am. Chem. Soc.* **1982**, *104*, 1095.
(11) Etter, M. C. *Acc. Chem. Res.* **1990**, *23*, 120.
(12) Whitesell, J. K.; Davis, R. E.; Saunders, L. L.; Wilson, R. J.; Feagins, J. P. *J. Am. Chem. Soc.* **1991**, *113*, 3267.
(13) Harrison, W. T. A.; Nenoff, T. M.; Gier, T. E.; Stucky, G. D. *Inorg. Chem.* **1993**, *32*, 2437.
(14) SMART Program; Bruker AXS, Inc.: Madison, WI, 1996.
(15) SAINTPLUS; Bruker AXS, Inc.: Madison, WI, 1996.
(16) Betteridge, P. W.; Carruthers, J. R.; Cooper, R. I.; Prout, C. K.; Watkin, D. J. *J. Appl. Crystallogr.* **2003**, *36*, 1487.
(17) Sheldrick, G. M. SHELXS86. In *Crystallographic Computing 3*; Sheldrick, G. M., Kruger, C., Goddard, R., Eds.; Oxford University Press: Oxford, U.K., 1985; pp 175−189.
(18) Beurskens, P. T.; Admiraal, G.; Beurskens, G.; Bosman, W. P.; de Gelder, R.; Israel, R.; Smits, J. M. M. The DIRDIF_94 program system; Technical Report of the Crystallographic Laboratory; University of Nijmegen: Nijmegen, The Netherlands, 1994.
(19) SADABS: Area-Detector Absorption Correction; Siemens Industrial Automation, Inc.: Madison, WI, 1996.
(20) Halasyamani, P. S.; Poeppelmeier, K. R. *Chem. Mater.* **1998**, *10*, 2753.
(21) Halasyamani, P. S. *Chem. Mater.* **2004**, *16*, 3586.
(22) Shahriari, D. Y.; Barnabe, A.; Mason, T. O.; Poeppelmeier, K. R. *Inorg. Chem.* **2001**, *40*, 5734.
(23) Shahriari, D. Y.; Erdman, N.; Haug, U. T. M.; Zaryczny, M. C.; Marks, L. D.; Poeppelmeier, K. R. *J. Phys. Chem. Solids* **2003**, *64*, 1437.
(24) Sheets, W. C.; Mugnier, E.; Barnabe, A.; Marks, T. J.; Poeppelmeier, K. R. *Chem. Mater.* **2006**, *18*, 7.
(25) Ballhausen, C. J.; Gray, H. B. *Inorg. Chem.* **1962**, *1*, 111.
(26) Welk, M. E.; Norquist, A. J.; Stern, C. L.; Poeppelmeier, K. R. *Inorg. Chem.* **2000**, *39*, 3946.
(27) Welk, M. E.; Norquist, A. J.; Arnold, F. P.; Stern, C. L.; Poeppelmeier, K. R. *Inorg. Chem.* **2002**, *41*, 5119.
(28) Du, L. S.; Schurko, R. W.; Kim, N.; Grey, C. P. *J. Phys. Chem. A* **2002**, *106*, 7876.
(29) Withers, R. L. *Ferroelectrics* **2004**, *305*, 69.

CG0609062